Final state-selected spectra in unimolecular reactions: A transition-state-based random matrix model for overlapping resonances

Uri Peskin and William H. Miller
Department of Chemistry, University of California, and Chemical Sciences Division, Lawrence Berkeley Laboratory, Berkeley, California 94720

Hanna Reisler
Department of Chemistry, University of Southern California, Los Angeles, California 90089-0482

(Received 26 September 1994; accepted 13 February 1995)

Final state-selected spectra in unimolecular decomposition are obtained by a random matrix version of Feshbach's optical model. The number of final states which are independently coupled to the molecular quasibound states is identified with the number of states at the dividing surface of transition state theory (TST). The coupling of the transition state to the molecular complex is modeled via a universal random matrix effective Hamiltonian which is characterized by its resonance eigenstates and provides the correct average unimolecular decay rate. The transition from nonoverlapping resonances which are associated with isolated Lorentzian spectral peaks, to overlapping resonances, associated with more complex spectra, is characterized in terms of deviations from a χ^2-like distribution of the resonance widths and the approach to a random phase-distribution of the resonance scattering amplitudes. The evolution of the system from a tight transition state to reaction products is treated explicitly as a scattering process where specific dynamics can be incorporated. Comparisons with recently measured final state-selected spectra and rotational distributions for the unimolecular reaction of NO_2 show that the present model provides a useful new approach for understanding and interpreting experimental results which are dominated by overlapping resonances.

I. INTRODUCTION

Transition-state-based statistical theories (e.g., RRKM) have been successful in describing the unimolecular reactions of a large number of molecules, especially under conditions of extensive averaging, e.g., over initial reactant states and final product states. In the last decade, however, it has become possible to study unimolecular decomposition of small molecules under conditions of monochromatic excitation and state-specific product detection.[1] For small molecules, even when IVR is complete, averaging is intrinsically less extensive and it is possible to observe, under favorable conditions, quantities for which only the average values have heretofore been available. For example, the distribution of state-specific decay rates about the statistical average has been observed experimentally for formaldehyde in the tunneling regime and compared with the predictions of a random matrix model and transition state theory (TST).[2]

For most dissociating molecules above the tunneling regime (i.e., when the excitation energy is well above the dissociation threshold), the coupling between the molecular complex and the continuum is strong and the density of strongly mixed molecular states is large, so that the unimolecular decay is characterized by overlapping resonance states. These states are associated with complex energies $\{E_l - i\Gamma_l/2\}$ which are the eigenvalues of the time-independent Schrödinger equation with outgoing wave boundary conditions (Siegert eigenvalues).[3] The resonances are overlapping when the average resonance width $\langle\Gamma\rangle$ is larger than the average energy spacing between resonances ΔE, i.e.,

$$\frac{\langle\Gamma\rangle}{\Delta E} = \langle\Gamma\rangle\rho > 1. \tag{1.1}$$

(These averages are with respect to a set of strongly mixed metastable states in a relatively narrow energy region characterized by the density of molecular states ρ.) Simple estimates of state densities and widths demonstrate that overlapping resonances are prevalent under typical conditions treated by TST/RRKM, especially in bond fission reactions with loose transition states. For NO_2 one has $\langle\Gamma\rangle\rho \approx 1-10$ at excess energies between 5 and 2000 cm^{-1}.[4,5] For NCNO near threshold, $\langle\Gamma\rangle \approx 0.1\ cm^{-1}$ and $\rho \approx 300/cm^{-1}$,[6] and thus $\langle\Gamma\rangle\rho \approx 30$, exhibiting even stronger overlap. For larger molecules, the resonances always overlap except at energies very near dissociation threshold.

Until recently no clear experimental demonstration of overlapping resonances in unimolecular reactions existed, but in a series of experiments on the unimolecular reaction of expansion-cooled NO_2 at excess energies from 0 to 3030 cm^{-1}, it was observed that the spectral features obtained by monitoring selected final states while scanning the photolysis energy are different not only in their intensity but also in line shapes and positions.[4,7–10] Such final state selected spectra, also known as photofragment yield (PHOFRY) or photofragment excitation (PHOFEX) spectra,[1] provide a sensitive tool for studying unimolecular decomposition and can reveal features relating to resonance overlap and the nature of the transition state.[7,8] Reisler and co-workers suggested that the state-specific photofragment yield spectra are a manifestation of the so called ''Ericson fluctuations'' in nuclear reactions.[7,8] Ericson proposed that in the case of overlapping resonances the cross sections into specific final states will

 0021-9606/95/102(22)/8874/13/$6.00

fluctuate as a function of energy and these fluctuations will not diminish with increasing excess energy (provided that the density of states is not too high), but rather become more random.[11]

The interpretation of the final-state selected spectra, however, is not always a simple task. When the coupling between each metastable molecular state and the continuum into which it decays is weak, the spectra are well characterized by Lorentzian line shapes,

$$P(E)\approx \text{const}\left|\frac{1}{E-E_l+i\Gamma_l/2}\right|^2, \tag{1.2}$$

each corresponding to an exponentially decaying resonance (quasibound) state. The energy of the quasibound state, E_l, defines its spectral location along the energy axis, and the width of the Lorentzian peak corresponds to the decay rate of that state,

$$k_l=\Gamma_l/\hbar. \tag{1.3}$$

This clear and well established picture holds as long as the resonances are isolated (or nonoverlapping), i.e., when

$$\langle\Gamma\rangle\rho<1. \tag{1.4}$$

When the resonances overlap, isolated Lorentzian peaks are not observed, and the Siegert eigenvalues are not related to the spectrum in a direct fashion.[12] Therefore, a more detailed analysis of the final state-selected spectra is needed in order to gain insight into the unimolecular decay mechanism. For typical optical excitation, the probability of observing a final state j at energy E is given within the Franck–Condon dipole approximation as

$$P_j(E)=|\mu\langle\Phi_0|\psi_j,E\rangle|^2, \tag{1.5}$$

where E is the excess energy above the dissociation threshold, $|\Phi_0\rangle$ is the nuclear ground state of the molecule, and μ is the electronic transition dipole matrix element. $|\psi_j,E\rangle$ is an exact continuum eigenstate of the molecular (nuclear) Hamiltonian whose asymptotic wave function $|j,E\rangle$ represents the free fragments.

The purpose of the present work is to introduce a simple model based on a random matrix version of Feshbach's optical model[13] for simulating final state-selected spectra in unimolecular reactions in cases of both isolated and overlapping resonances. Such a model is especially useful when accurate potential energy surfaces (PES) for the reaction are unavailable and exact dynamical calculations are beyond reach. The random matrix version of Feshbach's optical model, which will be described in detail here, was recently shown to be consistent with TST in simulating correctly the average unimolecular decay rates in the regimes of isolated and overlapping resonances alike.[14] Unlike the TST decay rate, the final state-selected spectra depend also on the evolution of the system beyond the transition state dividing surface towards the free products. We, therefore, modified the standard optical model by introducing ''dynamical'' coupling matrix elements that explicitly account for that evolution. This mixed approach combines a universal statistical description of the molecular complex with a reaction-specific dynamical description of the propagation from the transition state to the products.

The general formulation of the TST-based optical model and its application to simulate final state-selected spectra is first presented in Sec. II. The special case of a ''loose'' transition state (resembling product states) is discussed in Sec. III, and then applied to a triatomic molecule resembling the unimolecular decay of NO_2 near dissociation threshold. In particular, final state selected spectra are shown for varying degrees of overlap and compared qualitatively with experimental results. In Sec. IV, ''tight'' transition states are considered, and the specific case of a bond fission reaction of a triatomic molecule over a barrier is discussed in some detail. Illustrative examples of final state distributions are given for this model system. Finally, in Sec. V we present concluding remarks regarding the generality of the results and their relationship to experimental observations.

II. A TST-BASED RANDOM MATRIX OPTICAL MODEL

A. General formalism

Within the Franck–Condon approximation [Eq. (1.5)], the nuclear wave function of the metastable excited molecule is initially localized in the bound region of the molecular ground state (the Franck–Condon region). Therefore, it is sufficient to evaluate the scattering wave function $|\psi_j,E\rangle$ only in this region. A useful approach for this purpose is the Feshbach–Löwdin partitioning of Hilbert space into two complementary subspaces spanned by two orthogonal projection operators, P and Q ($P+Q=I$, $PP=P$, $QQ=Q$, $PQ=QP=0$).[13] Q is defined by a set of basis functions which span the bound-state space, and P projects onto the dissociative continuum to which it is coupled and decays. The projection of $|\psi_j,E\rangle$ onto the Q space is rigorously given in terms of a ''Lippman–Schwinger'' equation with an effective Hamiltonian,[13] i.e.,

$$Q|\psi_j,E\rangle=\frac{1}{E-H^{\text{eff}}(E)}\,QHP|j,E\rangle, \tag{2.1}$$

where H is the full (nuclear) Hamiltonian, and $H^{\text{eff}}(E)$ is a non-Hermitian Q-space operator, defined as

$$H^{\text{eff}}(E)=QHQ+\lim_{\epsilon\to 0}\,QHP\,\frac{1}{E+i\epsilon-PHP}\,PHQ. \tag{2.2}$$

In order to simulate the final state-selected spectra we first adopt the standard random matrix representation of the effective Hamiltonian.[2,15,16] Assuming that M molecular states, $\{|m>\}$, in the Q space are strongly mixed (ergodic), the effective Hamiltonian matrix is given by

$$[\mathbf{H}^{\text{eff}}(E)]_{m,m'}=E_m\delta_{m,m'}-i\pi\sum_{j=1}^{N_j}\langle m|H|j,E\rangle \times\langle j,E|H|m'\rangle, \tag{2.3}$$

for $m,m'=1,\ldots,M$. The E_m values are chosen from a Wigner distribution of nearest neighbor level spacings,[17]

$$f(S_m)=\frac{\pi S_m}{2\langle S_m\rangle^2}\, e^{-(\pi S_m^2/4\langle S_m\rangle^2)}, \tag{2.4a}$$

where the spacings are defined as $S_m=E_m-E_{m-1}$. The average spacing is associated with the density of strongly mixed molecular states

$$\langle S_m\rangle\equiv\Delta E=\frac{1}{\rho}, \tag{2.4b}$$

and W is the average energy range covered by the M molecular states,

$$W=\frac{M}{\rho}=M\langle S_m\rangle. \tag{2.4c}$$

We denote by N_j the number of final states $\{|j,E\rangle\}$ which are energetically accessible (i.e., the number of open channels), and it is assumed in the present version of the random matrix model that all open channels are independently coupled to the states in the Q-space. The coupling matrix elements between each final state and the molecular states, i.e. $\{\langle j,E|H|m\rangle\}$, are taken to be real and energy independent, which is not a severe approximation if the energy range W is sufficiently narrow. The effective Hamiltonian matrix can therefore be written as

$$(\mathbf{H}^{\rm eff})_{m,m'}=E_m\delta_{m,m'}-i\pi\sum_{j=1}^{N_j} v_{m,j}v_{m',j}, \tag{2.5a}$$

with

$$v_{m,j}\equiv\langle j,E|H|m\rangle. \tag{2.5b}$$

Within the ''ergodic'' (complete IVR) model, the coupling matrix elements are chosen from a Gaussian (normal) distribution with the standard deviation σ and a mean value 0, such that

$$\langle v_{j,m}v_{j',m'}\rangle=\delta_{m,m'}\delta_{j,j'}\sigma^2, \tag{2.5c}$$

where $\langle\cdots\rangle$ stands for the statistical average.[14] Other choices of the coupling matrix elements which avoid the complete IVR assumption are also possible[14,16(b)] but will not be considered here.

The effective Hamiltonian matrix is complex symmetric (non-Hermitian) and therefore its eigenvalues are complex, $\{E_l-i\Gamma_l/2\}$. The corresponding eigenvectors are the resonance states of the system. In the case of isolated resonances (the weak coupling limit, $\sigma\to 0$) these states characterize the unimolecular decay process in terms of Lorentzian spectral line shapes [Eq. (1.2)], and also provide the average unimolecular decay rate, k, via Eq. (1.3),[14] i.e.

$$\bar{k}=\frac{\bar{\Gamma}}{\hbar}, \tag{2.6}$$

where $\bar{\Gamma}$ is the average resonance width for a given realization of the effective Hamiltonian matrix,

$$\bar{\Gamma}=\frac{1}{M}\sum_{l=1}^{M}\Gamma_l=\frac{-2}{M}\,\mathrm{tr}[\mathrm{Im}(\mathbf{H}^{\rm eff})]=\frac{2\pi}{M}\sum_{m=1}^{M}\sum_{j=1}^{N_j}v_{m,j}^2. \tag{2.7a}$$

Averaging $\bar{\Gamma}$ over the distribution of coupling matrix elements [Eq. (2.5c)] gives

$$\langle\bar{\Gamma}\rangle=2\pi\sigma^2N_j. \tag{2.7b}$$

When the resonances overlap, however, the average unimolecular decay rate is not related to the average resonance width in such a simple fashion as in Eq. (2.6). In a recent paper,[14] we have given a TST interpretation to the optical model which predicts quite accurately the actual (simulated) decay rates of randomly chosen states in the Q space for both isolated and overlapping resonances. Within this interpretation, the number of states which are independently coupled to the Q space is identified with N, the number of energetically (classically) accessible states of the activated complex (the molecule with the reaction coordinate degree of freedom removed[18]) at the transition state dividing surface. The effective Hamiltonian takes the form (see Ref. 14)

$$(\mathbf{H}^{\rm eff})_{m,m'}=E_m\delta_{m,m'}-i\pi\sum_{n=1}^{N} V_{m,n}V_{m',n}, \tag{2.8}$$

and the TST expression for the decay rate associated with this effective Hamiltonian is[14]

$$\langle k_{\rm TST}\rangle=\frac{N}{2\pi\rho\hbar}\,\langle P\rangle, \tag{2.9a}$$

where $\langle P\rangle$ is the average transmission probability per state at the dividing surface,

$$\langle P\rangle=1-e^{-4\pi^2\sigma^2\rho}=1-e^{-2\pi\langle\bar{\Gamma}\rangle\rho/N}. \tag{2.9b}$$

The TST-dividing surface is associated with the point of local minimum flux along the reaction coordinate, and the number of states of the activated complex, N, is typically smaller than the number of final states for a given total energy, i.e.,

$$N\leqslant N_j, \tag{2.10}$$

equality maintaining in the limit of a ''loose transition state,'' where the point of minimal flux is in the asymptotic region. The other limiting case, $N\ll N_j$ refers to a ''tight transition state'' and is usually associated with a reaction barrier.[18]

To maintain consistency with the TST result for the average decay rate, the standard effective Hamiltonian [Eq. (2.5a)] should be replaced by the TST-based effective Hamiltonian [Eq. (2.8)]. This can be done rigorously according to the following derivation. Let us first introduce a set of N activated complex states, $\{|n,E\rangle\}$. Each state is associated with a total energy E, a set of good quantum numbers, n, for its ''internal'' degrees of freedom (i.e., excluding the reaction coordinate), and a free (separable) motion towards the ''products'' along the reaction coordinate. $\{|n,E\rangle\}$ are therefore the eigenstates of the full nuclear Hamiltonian at the dividing surface, defined by a fixed value of the reaction coordinate on the potential energy surface. Our derivation starts with the asymptotic completeness assumption; i.e., we assume that each final state $|j,E\rangle$ is obtained asymptotically from the time evolution of the set of N intermediate states at the TST dividing surface. This formally reads

$$\lim_{t\to\infty} e^{-iEt/\hbar}|j,E\rangle = \lim_{t\to\infty} \sum_{n=1}^{N} a_{j,n}(E) e^{-iHt/\hbar}|n,E\rangle. \quad (2.11)$$

It is convenient to rewrite Eq. (2.11) in terms of a Möller wave operator[12]

$$|j,E\rangle = \sum_{n=1}^{N} a_{j,n}(E)\hat{\Omega}(E)|n,E\rangle, \quad (2.12a)$$

where the Möller operator is defined as

$$\hat{\Omega}(E) = \lim_{t\to\infty} e^{+iEt/\hbar} e^{-iHt/\hbar}. \quad (2.12b)$$

Making use of Eq. (2.12) for the final states, we can rewrite the original effective Hamiltonian matrix [Eq. (2.3)] as

$$[\mathbf{H}^{\text{eff}}(E)]_{m,m'} = E_m \delta_{m,m'} - i\pi \sum_{j=1}^{N_j} \sum_{n=1}^{N} \sum_{n'=1}^{N} \times\langle m|H\hat{\Omega}(E)|n,E\rangle a_{j,n}(E) a^*_{j,n'}(E) \times\langle n',E|\hat{\Omega}^{\dagger}(E)H|m'\rangle, \quad (2.13)$$

which can be simplified by assuming asymptotic completeness for the final states; i.e., each intermediate state evolves asymptotically in time to the set of N_j final states

$$\lim_{t\to\infty} e^{-i\hat{H}t/\hbar}|n,E\rangle = \lim_{t\to\infty} \sum_{j=1}^{N_j} b_{n,j}(E) e^{-iEt/\hbar}|j,E\rangle, \quad (2.14)$$

or, in terms of the Möller operator

$$|n,E\rangle = \sum_{j=1}^{N_j} b_{n,j}(E)\hat{\Omega}^{\dagger}(E)|j,E\rangle. \quad (2.15)$$

Using Eqs. (2.12), (2.15) one has

$$b_{n,j}(E) = \langle j,E|\hat{\Omega}(E)|n,E\rangle = a^*_{j,n}(E). \quad (2.16)$$

Multipling Eq. (2.15) from the left by $\langle n',E|$ and using Eq. (2.16), one obtains the isometry of the Möller operator, i.e.,[12]

$$\delta_{n,n'} = \sum_{j=1}^{N_j} b_{n,j}(E) b^*_{n',j}(E) = \sum_{j=1}^{N_j} a^*_{j,n}(E) a_{j,n'}(E), \quad (2.17)$$

which, when used in Eq. (2.13), gives

$$[\mathbf{H}^{\text{eff}}(E)]_{m,m'} = E_m \delta_{m,m'} - i\pi \sum_{n=1}^{N} \langle m|H\hat{\Omega}(E)|n,E\rangle \times\langle n,E|\hat{\Omega}^{\dagger}(E)H|m'\rangle. \quad (2.18)$$

The effective Hamiltonian in Eq. (2.18) is expressed in terms of coupling matrix elements between the molecular states, $\{|m\rangle\}$, and N specific linear combinations of the final states, each one given by $\hat{\Omega}(E)|n,E\rangle$ for $n=1,\ldots,N$. The crucial assumption in our derivation is that the random matrix assumptions are imposed on these coupling matrix elements, i.e., we identify Eq. (2.18) with Eq. (2.8), where

$$V_{m,n} \equiv \langle m|H\hat{\Omega}(E)|n,E\rangle, \quad (2.19)$$

are assumed to be energy independent, real, and normally distributed around 0 with a standard deviation σ. Within the random matrix assumptions, Eq. (2.18) is identical to Eq. (2.5a) with N_j replaced by N. The physical basis for the present assumption is that the molecular states are strongly mixed (i.e., correspond to ergodic motion in the classical limit) only from the reactant Franck–Condon region to the transition state dividing surface.

B. Final state-selected spectra

An explicit expression for the final state-selected spectra can be written in terms of the effective Hamiltonian matrix. By using Eq. (2.1) and Eq. (2.12a) in Eq. (1.5) for the final state-selected probability, we obtain

$$P_j(E) = \left| \mu\langle\Phi_0|(E-H^{\text{eff}})^{-1}QHP \times\sum_{n=1}^{N} a_{j,n}(E)\hat{\Omega}(E)|n,E\rangle \right|^2. \quad (2.20)$$

Within the finite basis set representation of the effective Hamiltonian matrix as given in Eqs. (2.8), (2.19), Eq. (2.20) can be rewritten as

$$P_j(E) = \left| \mu \sum_{m=1}^{M} \Phi_{0,m} \sum_{m'=1}^{M} [(E\mathbf{I}-\mathbf{H}^{\text{eff}})^{-1}]_{m,m'} \times\sum_{n=1}^{N} a_{j,n}(E) V_{m',n} \right|^2, \quad (2.21)$$

where $\mathbf{H}^{\text{eff}}$ is the effective Hamiltonian matrix, and $\Phi_{0,m}$ ($\equiv\langle\Phi_0|m\rangle$) is the projection of the initial state onto the molecular state $|m\rangle$. Without loss of generality, we shall assume that the molecular basis states are excited uniformly, such that $\Phi_{0,m} = 1/\sqrt{M}$. As seen from Eq. (2.21), $P_j(E)$ depends on the random matrix elements $\{V_{m',n}\}$ for the coupling between the molecular states and the activated complex, and on "dynamical" matrix elements $\{a_{j,n}(E)\}$ for the coupling between the activated complex and the dissociation products. The present approach combines, therefore, a universal statistical description of the molecular system and a molecule-specific dynamical description of the propagation from the transition state to the products. We shall come to this point again later.

It is useful to rewrite Eq. (2.21) in terms of the resonance eigenvalues and eigenvectors of the effective Hamiltonian. By diagonalizing the effective Hamiltonian matrix numerically one has,

$$[(E\mathbf{I}-\mathbf{H}^{\text{eff}})^{-1}]_{m,m'} = \sum_{l} \frac{u^l_m u^l_{m'}}{E-E_l+i\Gamma_l/2}, \quad (2.22)$$

where $\{\mathbf{u}^l\}$ are the eigenvectors of $\mathbf{H}^{\text{eff}}$ associated with the (complex) resonance eigenvalues $\{E_l - i\Gamma_l/2\}$. Note that since $\mathbf{H}^{\text{eff}}$ is a complex symmetric matrix, its right and left

eigenvectors are identical (i.e., the left vector is not the complex conjugate of the right vector).[19] By substituting Eq. (2.22) into Eq. (2.21), the standard representation of the spectrum as a summation over Lorentzian-amplitudes with complex coefficients is obtained,

$$P_j(E)=\left|\sum_l \frac{C_j^l(E)e^{i\phi_j^l(E)}}{E-E_l+i\Gamma_l/2}\right|^2. \tag{2.23a}$$

The complex coefficients, which are characterized by their real amplitudes $\{C_j^l(E)\}$ and phases $\{\phi_j^l(E)\}$, are given by

$$C_j^l(E)e^{i\phi_j^l(E)}=\mu\sum_{m=1}^{M}\Phi_{0,m}u_m^l\sum_{m'=1}^{M}u_{m'}^l\sum_{n=1}^{N}a_{j,n}(E)V_{m',n}. \tag{2.23b}$$

We end this section by considering some limitations on the inputs of the model for the effective Hamiltonian. The input parameters are the density of molecular states ρ, the energy range W, the number of independent open channels N, and the coupling strength σ. The dimension of Q, $M=\rho W$, should be taken large enough to provide statistically meaningful results. For a fixed M, the minimal value of W should be of the order of the maximal resonance width, such that all the resonance widths will be sampled correctly within the energy range. This condition implies that (see Ref. 14)

$$\langle\Gamma\rangle\rho<N. \tag{2.24}$$

An upper bound for W is usually imposed by the physical conditions. The application of the model is limited to an energy range W for which the effective Hamiltonian is energy independent and ρ, σ, N_j, and N can reasonably assumed to be constants.

III. "LOOSE" TRANSITION STATES

We first consider the limiting case of a loose transition state where the activated complex is associated with an asymptotic value of the reaction coordinate. Physically, this case corresponds to the ergodic evolution of the excited molecule from the Franck–Condon region to the asymptotic final states (products). Such a transition state is invoked, for example, in the phase space theory (PST) of unimolecular decay.[20] The probability of obtaining a specific final state j at a given energy, should, therefore, be *independent of the identity* of this state. Within the random matrix optical model, all the open channels are independently and randomly coupled to the molecular states (i.e., the Q-space), so that

$$N\equiv N_j. \tag{3.1}$$

The TST interpretation of the model implies that the final states are identified with the states of the activated complex. In this case, therefore, the "dynamical" coupling matrix elements $a_{n,j}$ as defined in Eq. (2.16) are a Kronecker delta

$$a_{j,n}(E)=\delta_{j,n}. \tag{3.2}$$

By substituting Eqs. (3.1), (3.2) into Eq. (2.23), the expression for the final state-selected spectra for a loose transition state is obtained,

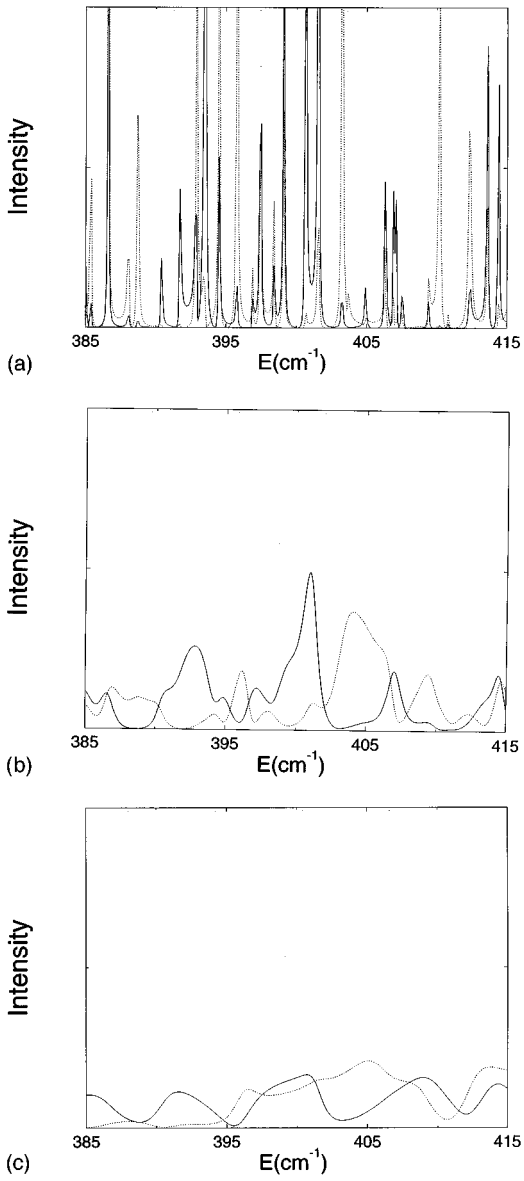

FIG. 1. (a) Final state-selected spectra $P_j(E)$ for $j=1$ (solid line) and $j=3$ (dashed line). The effective Hamiltonian parameters are $\rho=1$ cm^{-1}, $M=800$, $N=N_j=16$ and an average resonance width $2\pi\sigma^2N=0.1$. (b) The same for $2\pi\sigma^2N=2.0$. (c) The same for $2\pi\sigma^2N=10.0$.

$$P_j(E)=\left|\sum_l \frac{C_j^l e^{i\phi^l}}{E-E_l+i\Gamma_l/2}\right|^2, \tag{3.3a}$$

where the complex coefficients are energy-independent and are statistically identical for all the final states $\{j\}$,

$$C_j^l e^{i\phi^l}=\mu\sum_{m=1}^{M}\Phi_{0,m}u_m^l\sum_{m'=1}^{M}u_{m'}^l V_{m',j}. \tag{3.3b}$$

Equation (3.3) implies that $P_j(E)$ depends only on the effective Hamiltonian matrix and not on any exit channel dynamics.

In Fig. 1 typical spectra are presented, which illustrate the transition from the weak coupling (nonoverlapping) regime to the strong coupling (overlapping) regime. When the

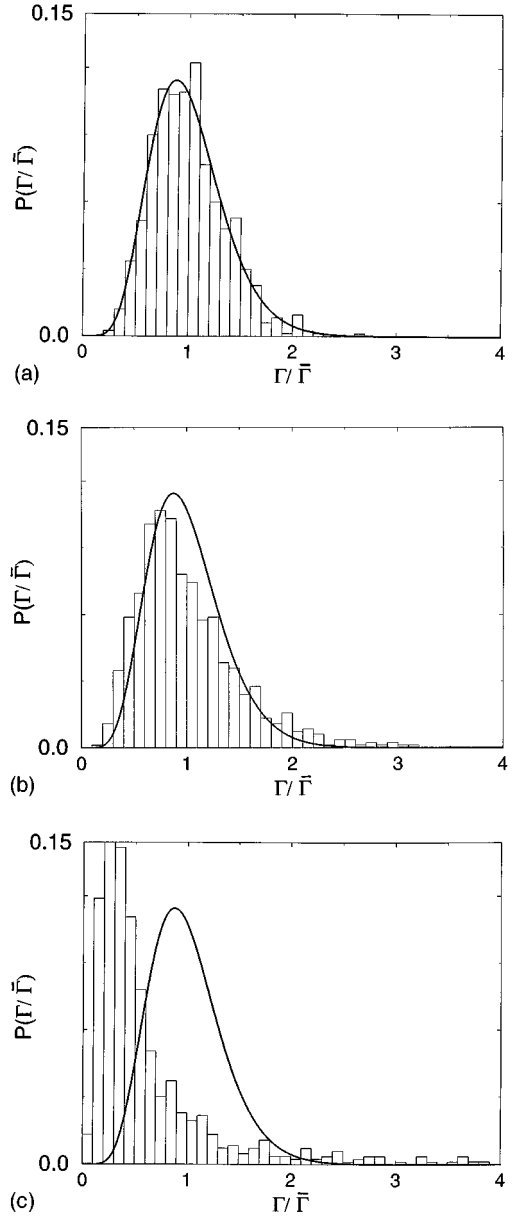

FIG. 2. (a) Solid line, χ^2 distribution function with 16 degrees of freedom. The histograms represent the probability distribution of the normalized resonance widths ($\Gamma/\bar{\Gamma}$) as obtained by diagonalizing the effective Hamiltonian, with the parameters of Fig. 1(a). (b) The same, for the parameters of Fig. 1(b). (c) The same, for the parameters of Fig. 1(c).

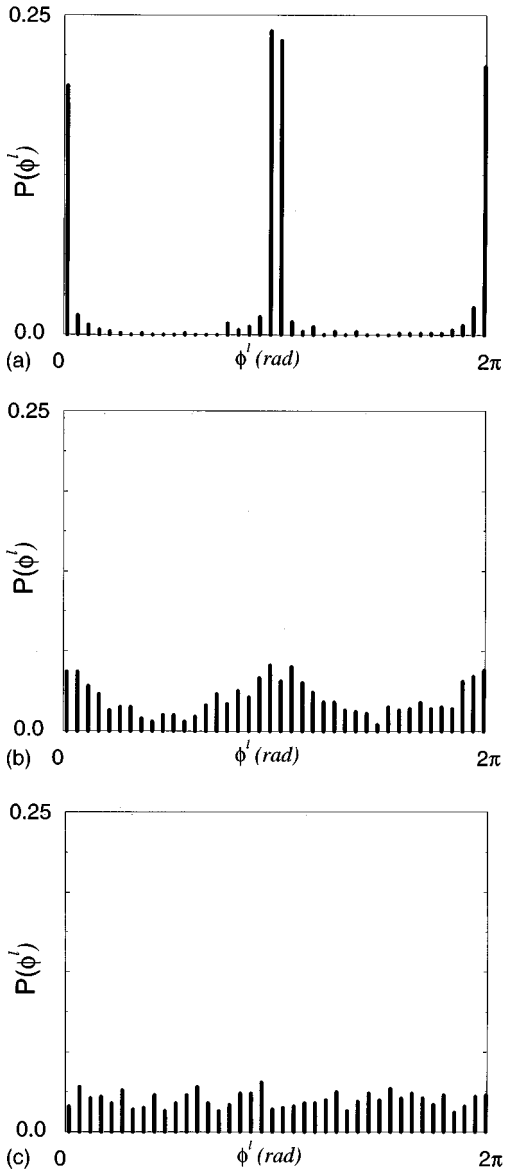

FIG. 3. (a) Probability distribution of the phases, ϕ^l, as defined by Eq. (3.3b) for the effective Hamiltonian with the parameters of Fig. 1(a). (b) The same, for the parameters of Fig. 1(b). (c) The same, for the parameters of Fig. 1(c).

degree of resonance overlap is small [$\langle\bar{\Gamma}\rangle\rho=0.1$ as in Fig. 1(a)], Lorentzian peaks are observed and the spectra for different j states have different intensities, but similar line positions and widths. As the overlap increases [Figs. 1(b) and 1(c)], the peaks are shifted, mixed, and broadened, and the spectra for different j states begin to differ also in their line positions and widths, a result of state-specific interference between the resonance amplitudes. The behavior shown in Figs. 1(b) and 1(c) is qualitatively similar to that observed in the state-selected spectra obtained for NO_2 in the near threshold region[4] and at $E=2000-2500$ cm^{-1}, respectively.[8]

Figure 2 shows the distributions of resonance widths that are associated with each spectrum in Fig. 1. In the nonoverlapping regime the distribution of state-specific unimolecular decay rates (and also resonance widths) is expected to be χ^2-like with N degrees of freedom, according to the ''Golden Rule'' (perturbative) limit of the random matrix model,[2,21] and indeed this is found in our simulations as illustrated in Fig. 2(a). As the overlap increases, not only does the average width increase, but the distribution of widths increasingly deviates from a χ^2-like distribution. The deviations are associated with an increasingly longer tail, as can be seen in Figs. 2(b), 2(c) [and see also Ref. 16(a)]. In Fig. 2, the bars represent the distribution obtained in the present simulations, while the solid line is the corresponding χ^2 distribution.

The shapes of the spectral features are directly related to the interference between different resonance amplitudes.[8,11] The interference is well characterized in terms of the phases $\{\phi^l\}$ in Eq. (3.3). In Fig. 3 the distributions of phases which

correspond to the spectra in Fig. 1 are plotted. It is clear that in the weak coupling regime, the phases are strongly peaked around integer multiplies of π, indicating that the coefficients in Eq. (3.3b) (the residues) are approximately real. This is directly related to the fact that in this limit the resonance eigenvectors of the effective Hamiltonian, $\{\mathbf{u}^l\}$, are simply the zeroth basis $\{|m\rangle\}$ itself, i.e., $u^l_m \approx \delta_{l,m}$. As the coupling increases the coefficients become complex and eventually [see Fig. 3(c)] their phases become uniformly (and randomly) distributed between 0 to 2π, justifying a statistical treatment of overlapping resonances as is done in theories of nuclear reactions.[11,13] The random phases eventually result in the disappearance of the resonance structures in the spectra [see Fig. 1(c)], a result characteristic of dissociation in the strong coupling limit (e.g., a direct reaction).

Simulations such as the ones presented above provide a useful way of qualitatively interpreting experimentally measured spectra when dynamical calculations are computationally beyond reach and a statistical description of the process is justified. The spectra depend, via the effective Hamiltonian matrix, on three independent parameters; the molecular density of states ρ, the number of independent open channels N, and the average coupling strength between the P-space and the Q-space, σ. For a loose transition state, N is equal to the number of final states and is usually well known for a given energy. Therefore, a comparison between simulated and experimental spectra can be useful in estimating ρ, σ, and also the average unimolecular reaction rate via Eq. (2.9).

As an illustrative example consider the near-threshold unimolecular reaction of NO_2 at access energies 0–13 cm^{-1}. The NO state-selected spectra in this energy range were measured by Miyawaki *et al.*[4] Just above threshold, i.e., for access energies $0<E<5$ cm^{-1}, the number of independent open dissociation channels in $N=4$. The final state selected spectra are characterized by sharp peaks with an average width which is much smaller than 1 cm^{-1} (see Fig. 4 in Ref. 4). The average spectral width increases above 5 cm^{-1}, where another rotational state of NO opens up, so that the total number of open channels is $N=8$.[4] For the entire energy interval 0–13 cm^{-1}, the spectra obtained by monitoring *different* final NO quantum states exhibit differences in the positions, widths, and heights of the spectral features. However, each one of the two subintervals associated with $N=4$ and $N=8$ is characterized by a typical distribution of peak widths, and positions that are clustered around the zero-order states.

A quantitative peak-to-peak fitting of a random matrix simulation of the experimental measurements is neither possible nor is it the goal of the present work. Rather, a qualitative comparison of trends in the simulated and experimental spectra can be used to estimate the ranges of molecular parameters and aid in the interpretation of the experimental spectra. Near threshold, the number of open channels N is well defined (4 or 8 in the present case). From the molecular absorption spectrum just *below threshold*, we estimate the density of states ρ at 5–10 states per wave number.[4,5] Fixing $N=4$ and $\rho=6$ in the simulations, as well as the positions of the zero order states, we obtain final state selected spectra of different appearance by using different values of the resonance width parameter, $\langle\bar{\Gamma}\rangle=2\pi N\sigma^2$. For example, Figs. 4(a) and 4(b) correspond to $\langle\Gamma\rangle\rho=0.6$ and 3.0, respectively. In each figure, spectra of two different dissociation channels are presented [chosen arbitrarily as $j=1,2$ in Eq. (3.3a)]. Comparing the simulations to the experimental spectra in Ref. 4, we conclude by inspection that the spectra displayed in Fig. 4(b) fits better the experimental results in terms of the distribution of peak widths and overlap, and the dynamic range of the intensities (peak heights). Our simulations indicate that the decaying molecular complex is characterized by overlapping resonances, a fact that is reflected in the pronounced differences between spectra obtained when monitoring different open channels (in both the measured and simulated spectra). The degree of resonance overlap can be roughly estimated at $\langle\Gamma\rangle\rho\approx 3$, based on these simulations.

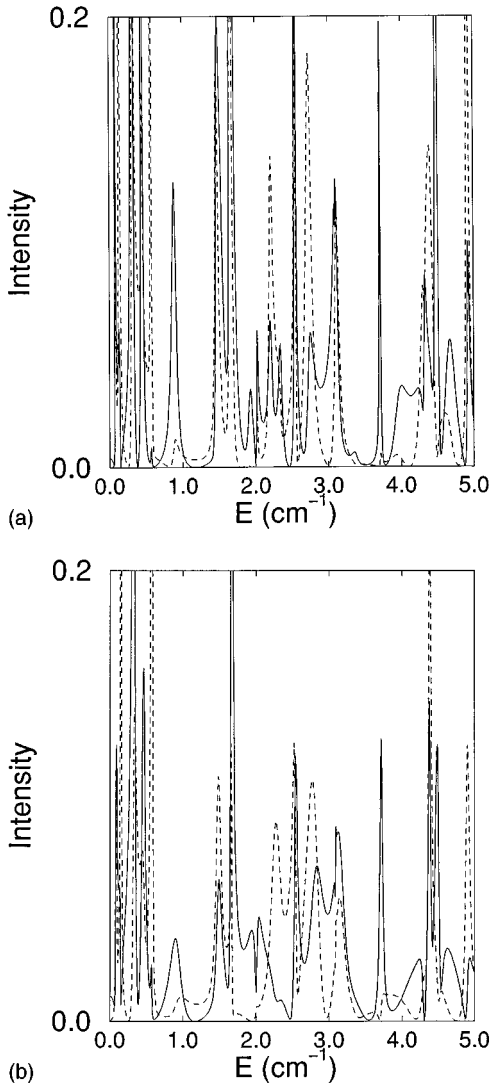

FIG. 4. (a) Simulated final state-selected spectrum $P_j(E)$ for $j=1$ (solid) and $j=2$ (dashed). The effective Hamiltonian parameters are $\rho=6/cm^{-1}$, $M=30$, $N=4$ and an average resonance width $2\pi\sigma^2N=0.1$. (b) The same for $2\pi\sigma^2N=0.5$.

In Fig. 5, simulated spectra for the range $5<E<13$ cm^{-1} are plotted, where σ and ρ are assumed to be the same as in the first energy interval. Compared to the plot in Fig.

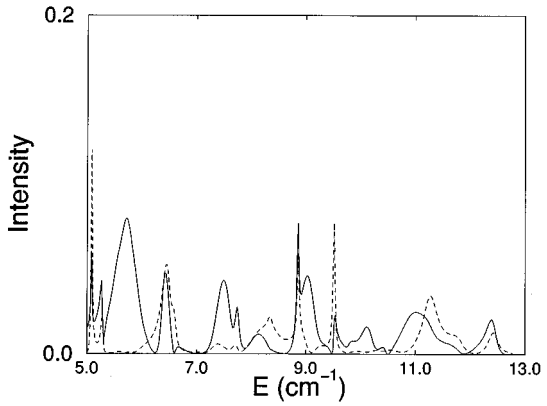

FIG. 5. Simulated final state-selected spectrum $P_j(E)$ for $j=1$ (solid) and $j=2$ (dashed). The effective Hamiltonian parameters are $\rho=6/\mathrm{cm}^{-1}$, $M=48$, $N=8$ and an average resonance width $2\pi\sigma^2 N=1.0$.

4(b), a reduction in average intensity and further broadening of the spectral features are obtained, in accord with the experimental observations.[4,8–10] The reduction in intensity in the state selected spectra at the higher energy range reflects the lower fractional population of each open channel. Note also that here again, in agreement with the degree of resonance overlap, different final state-selected spectra exhibit differences in spectral widths and peak positions.

The simulations also enable us to estimate the average unimolecular rate constant. The average width of the spectral features measured in this wavelength region is 0.1–0.2 cm^{-1}.[4] However, this value cannot be used directly to estimate the decay rate in the regime of overlapping resonances.[8] To estimate the near threshold rate we can use the density of states and the degree of resonance overlap, according to Eq. (2.9b). The average transmission probability is [see Eq. (2.9b)],

$$\langle P\rangle = 1-e^{-2\pi\times 3/4}\approx 0.99,$$

which is very close to the classical RRKM limiting result (i.e., $\langle P\rangle=1$). The average unimolecular decay width near threshold (i.e., for $N=4$) estimated according to Eq. (2.9a) is therefore

$$\hbar\langle k_{\mathrm{TST}}\rangle = \langle P\rangle\times\frac{4}{2\pi\times 6}\approx 0.105\ \ \mathrm{cm}^{-1},$$

which correspond to a decay rate of

$$\langle k_{\mathrm{TST}}\rangle = 0.0198\ \ \mathrm{ps}^{-1}.$$

IV. TIGHT TRANSITION STATES IN BOND FISSION REACTIONS

Tight transition states usually arise when a real barrier exists in the exit channel (e.g., due to avoided crossings[18,22]), or in the absence of a such a fixed barrier, when the point of minimum flux along the reaction coordinate is in the ''interior'' region of the potential surface.[23–25] Since such a transition state is associated with an energetic bottleneck along the reaction coordinate, the number of states of the activated complex is smaller than the number of asymptotic open channels, i.e.,

$$N < N_j. \tag{4.1}$$

Although we invoke a random matrix model for the evolution of the system from the Franck–Condon region to the transition state (assuming ergodic dynamics, i.e., strong mixing of the molecular states), the coupling of the transition state to the final states is evaluated explicitly, and thus the final states are identified within the model. As an example, we evaluate the dynamic coupling matrix elements and simulate the final state distributions for a simple specific case of a bond-fission reaction of a triatomic molecule ($ABC\rightarrow A+BC$).

A. Dynamical coupling matrix elements

We consider the photoinitiated unimolecular decomposition of a triatomic molecule $ABC\rightarrow A+BC$ with total angular momentum $J=0$ and total energy E. The PES in Jacobi coordinates is given in terms of the distance R between A and the BC center of mass, the angle θ between the bond axis of the diatom and the axis defined by A and the BC center of mass, and r, the BC distance. The molecular Hamiltonian for total $J=0$ is

$$H(R,r,\theta) = \frac{1}{2\mu_{A-BC}}\left(\frac{-\hbar^2}{R}\frac{\partial^2}{\partial R^2}R+\frac{\hat{j}^2}{R^2}\right) + \frac{1}{2\mu_{BC}}\left(\frac{-\hbar^2}{r}\frac{\partial^2}{\partial r^2}r+\frac{\hat{j}^2}{r^2}\right)+V(R,r,\theta), \tag{4.2}$$

where, as $R\rightarrow\infty$, $V(R,r,\theta)\rightarrow V_0(r)$. The asymptotic Hamiltonian defines the possible final states of the dissociation process. These are the rovibrational states of BC,

$$\langle R,r,\theta|\,\nu,j,E\rangle = Y_{j,0}(\theta)\phi_{\nu,j}(r)\chi_{\nu,j,E}(R), \tag{4.3a}$$

where the rotational functions are the spherical harmonics

$$\hat{j}^2 Y_{j,0}(\theta) = \hbar^2 j(j+1)Y_{j,0}(\theta), \tag{4.3b}$$

$\phi_{\nu,j}(r)$ are the vibrational functions which are the solutions of the asymptotic Schrödinger equation

$$\left\{\frac{\hbar^2}{2\mu_{BC}}\left[\frac{-1}{r}\frac{\partial^2}{\partial r^2}r+\frac{j(j+1)}{r^2}\right]+V_0(r)\right\}\phi_{\nu,j}(r) = E_{\nu,j}\phi_{\nu,j}(r), \tag{4.3c}$$

and $\chi_{\nu,j,E}(R)$ are the solutions of the radial equation in R,

$$\left\{\frac{\hbar^2}{2\mu_{A-BC}}\left[\frac{-1}{R}\frac{\partial^2}{\partial R^2}R+\frac{j(j+1)}{R^2}\right]\right\}\chi_{\nu,j,E}(R) = (E-E_{\nu,j})\chi_{\nu,j,E}(R). \tag{4.3d}$$

The transition state is defined by the center of mass coordinate $R=R_0$ along the PES (the dividing surface). It is assumed here that the motion along the dividing surface is uncoupled from the motion along the reaction coordinate from the transition state ($R=R_0$) to the product region ($R\rightarrow\infty$). The Hamiltonian at the transition state is therefore separable,

$$H^{\mathrm{TS}}(R,r,\theta) = H^{\ddagger}(r,\theta)+\frac{-\hbar^2}{2\mu_{A-BC}R}\frac{\partial^2}{\partial R^2}R, \tag{4.4a}$$

where $H^{\ddagger}(r,\theta)$ is the Hamiltonian of the activated complex (i.e., the molecule at the transition state with the reaction coordinate removed),

$$H^{\ddagger}(r,\theta)=\frac{1}{2\mu_{A-BC}}\frac{\hat{j}^2}{R_0^2}+\frac{1}{2\mu_{BC}}\left(\frac{-\hbar^2}{r}\frac{\partial^2}{\partial r^2}r+\frac{\hat{j}^2}{r^2}\right)+V(R_0,r,\theta). \tag{4.4b}$$

The intermediate states, $\{|n,E\rangle\}$, are the eigenstates of $H^{\ddagger}(r,\theta)$ [Eq. (4.4a)] defined as

$$\langle R,r,\theta|n,E\rangle=\Psi_n^{\ddagger}(r,\theta)\varphi_{n,E}^{\ddagger}(R), \tag{4.5}$$

where

$$H^{\ddagger}(r,\theta)\Psi_n^{\ddagger}(r,\theta)=E_n^{\ddagger}\Psi_n^{\ddagger}(r,\theta), \tag{4.6a}$$

and

$$\left(\frac{-\hbar^2}{2\mu_{A-BC}R}\frac{\partial^2}{\partial R^2}R\right)\varphi_{n,E}^{\ddagger}(R)=(E-E_n^{\ddagger})\varphi_{n,E}^{\ddagger}(R). \tag{4.6b}$$

An explicit expression for the dynamical coupling matrix elements is given in terms of the asymptotic (final) states and the activation complex states according to Eq. (2.16),

$$a_{(j,\nu),n}=\lim_{t\to\infty}\langle n,E|e^{-iEt/\hbar}e^{+iHt/\hbar}|\nu,j,E\rangle. \tag{4.7}$$

The right-hand side in the last equation can be calculated exactly by using numerical methods. One can propagate $|\nu,j,E\rangle$ in time as an initial wave packet,[22] or apply time-independent approaches to evaluate the limit in Eq. (4.7) in terms of a Green's operator. One can also apply simplifying approximations in order to estimate the dynamical coupling matrix elements. The crudest quantum mechanical approximation is the sudden approximation, which is justified whenever most of the energy E is associated with the motion along the reaction coordinate.[22,26] Within this approximation, the matrix elements reduce to

$$a_{(j,\nu),n}\approx 2\pi\int_0^{\pi}\sin(\theta)d\theta\int_{-\infty}^{\infty}r^2dr\Psi_n^{\ddagger}(r,\theta)\phi_{\nu,j}(r)Y_{j,0}(\theta), \tag{4.8}$$

which are the rovibrational Franck–Condon factors.[22,26,27]

A further simplification can be introduced when the excess energy of the molecular complex is not sufficient to excite the vibration of BC. In this case, BC can be approximated as a rigid rotor at the nuclear separation r_0. Repeating the derivation [Eqs. (4.2)–(4.8)] for this case, one has

$$a_{j,n}\approx 2\pi\int_0^{\pi}\sin(\theta)d\theta\Psi_n^{\ddagger}(\theta)Y_{j,0}(\theta)\equiv\langle\Psi_n^{\ddagger}|Y_{j,0}\rangle, \tag{4.9}$$

where $\{\Psi_n(\theta)\}$ are the eigenfunctions of the bending Hamiltonian $H^{\ddagger}(\theta)$,

$$H^{\ddagger}(\theta)\Psi_n^{\ddagger}(\theta)=E_n\Psi_n^{\ddagger}(\theta), \tag{4.10a}$$

and

$$H^{\ddagger}(\theta)=\frac{\hat{j}^2}{2\mu_{A-BC}R_0^2}+\frac{\hat{j}^2}{2\mu_{BC}r_0^2}+V(R_0,r_0,\theta). \tag{4.10b}$$

The coupling matrix elements $\{a_{j,n}\}$ can be readily obtained numerically by diagonalizing the matrix representation of $H^{\ddagger}(\theta)$ in a basis set of the spherical harmonics, i.e., Eq. (4.10a) can be rewritten as

$$\sum_{j'}\langle Y_{j,0}|H^{\ddagger}|Y_{j',0}\rangle\langle Y_{j',0}|\Psi_n^{\ddagger}\rangle=E_n\langle Y_{j,0}|\Psi_n\rangle; \tag{4.11}$$

or by using the definition in Eq. (4.9),

$$\sum_{j'}(\mathbf{H}^{\ddagger})_{j,j'}a_{j',n}^{*}=E_n a_{j,n}^{*}, \tag{4.12a}$$

where the bending Hamiltonian matrix is defined as

$$(\mathbf{H}^{\ddagger})_{j,j'}=\langle Y_{j,0}|H^{\ddagger}|Y_{j',0}\rangle=B_{\rm rot}^{\ddagger}j(j+1)\delta_{j,j'}+2\pi\int_0^{\pi}d\theta\,\sin(\theta)Y_{j,0}^{*}(\theta)V(R_0,r_0,\theta)Y_{j',0}(\theta), \tag{4.12b}$$

and the effective rotational constant at the transition state, $B_{\rm rot}^{\ddagger}$, is defined as

$$B_{\rm rot}^{\ddagger}=\frac{\hbar^2}{2\mu_{A-BC}R_0^2+2\mu_{BC}r_0^2}. \tag{4.12c}$$

According to Eq. (4.12a) the coupling matrix element $a_{j,n}$ is identified with the jth component of the nth eigenvector of the matrix $\mathbf{H}^{\ddagger}$.

B. Rotational state distributions

In the case of a tight transition state, the number of states of the activated complex in a given energy range (i.e., N) is usually unknown except for the fact that it is smaller than the actual number of open final channels [Eq. (4.1)]. Although random matrix simulations cannot provide a direct means for determining N for specific reactions, variational RRKM calculations have done so successfully in selected cases.[23–25] The random matrix model that we present here describes, however, the general dependence of the final state distributions on N (i.e., on excess energy). As an illustrative example we consider the model triatomic system for bond-fission reactions as described above. The transition state is characterized by a barrier height of 3000 cm^{-1} above the dissociation threshold and is located at $R_0=2.5$ Å. The diatom BC is modeled as a rigid rotor and the effective rotational constant [see Eq. (4.12c)] is taken as $B_{\rm rot}^{\ddagger}=2\ \mathrm{cm}^{-1}$. An anharmonic potential is assumed for the bending motion at the transition state,

$$V(R_0,r_0,\theta)\equiv v(\theta)=\sum_k C_k\cos^k(\theta). \tag{4.13}$$

In Fig. 6, the bending potential and the Hamiltonian eigenfunctions of the activated complex [obtained numerically according to Eq. (4.12)] are plotted.

Consider first the limiting case of a tight transition state with $N=1$. In this case all the asymptotic final states are obtained from a single intermediate state, i.e., the ground

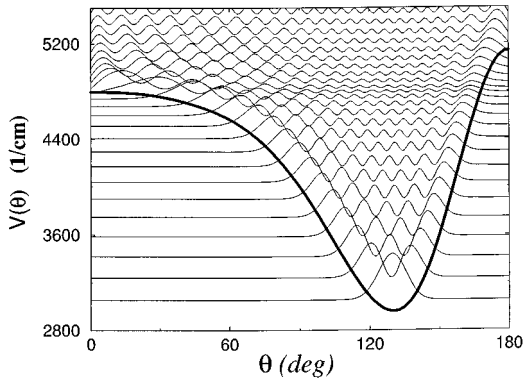

FIG. 6. Thick line, the bending potential at the transition state $v(\theta)$ as defined in Eq. (4.13). The expansion coefficients $\{C_k;\ k=0,\ldots,7\}$ are correspondingly given by 4000, 1600, −900, −230, 470, −760, 1400, −780 cm^{-1}. Thin lines, probability densities, $\mathrm{const}\times|\Psi_n(\theta)\sin(\theta)|^2$, for the eigenfunctions of the transition state (bending) Hamiltonian (the base lines correspond to the bending energies). The wave functions are obtained by diagonalizing the bending Hamiltonian in a basis of 80 spherical harmonics.

bending level of the activated complex. It is therefore expected that, irrespective of the excited resonance state(s), the distribution of final states will depend on the exit channel dynamics from that intermediate state. In the present model this implies that $N=1$ in Eq. (2.23). Within the sudden approximation the dynamical coupling matrix elements are energy independent [Eq. (4.9)] so that the state-selected probability [Eq. (2.23)] can be rewritten as

$$P_j(E)=|f(E)|^2\times|a_{j,1}|^2, \tag{4.14}$$

and consequently the final state distribution does not depend on excitation energy except for a j-independent factor, $|f(E)|^2$. This is illustrated in Fig. 7(a) for the model bond-fission reaction where the simulated rotational distributions are obtained according to Eq. (2.23) with $N=1$. The two different spectra are associated with two nearby energies separated by 2 cm^{-1}. Clearly, the two rotational distributions are identical (up to a constant factor). The observed fast oscillations as a function of j are well understood in this simple case,[28] and derive from the ''mapping'' (expansion coefficients) of the activated complex bending state in terms of the free rotor states.[22] (They are usually washed out when several initial parent states are populated.[22,28–30])

This simple picture breaks down, however, when N is larger, as illustrated in Fig. 7(b) for $N=8$. Here the envelopes of the rotational distributions associated with the two nearby energies are completely uncorrelated, and the oscillatory patterns of the distributions are not related to the expansion coefficients $\{a_{j,n}\}$ in a direct fashion. To interpret these observations, we express $P_j(E)$ in Eq. (2.23) as follows:

$$P_j(E)=\left|\sum_n g_n(E)a_{j,n}\right|^2, \tag{4.15a}$$

where

$$g_n(E)=\sum_l \frac{\mu}{E-E_l+i\Gamma_l/2}\sum_{m=1}^{M}\Phi_{0,m}u_m^l\sum_{m'=1}^{M}u_{m'}^l V_{m',n}. \tag{4.15b}$$

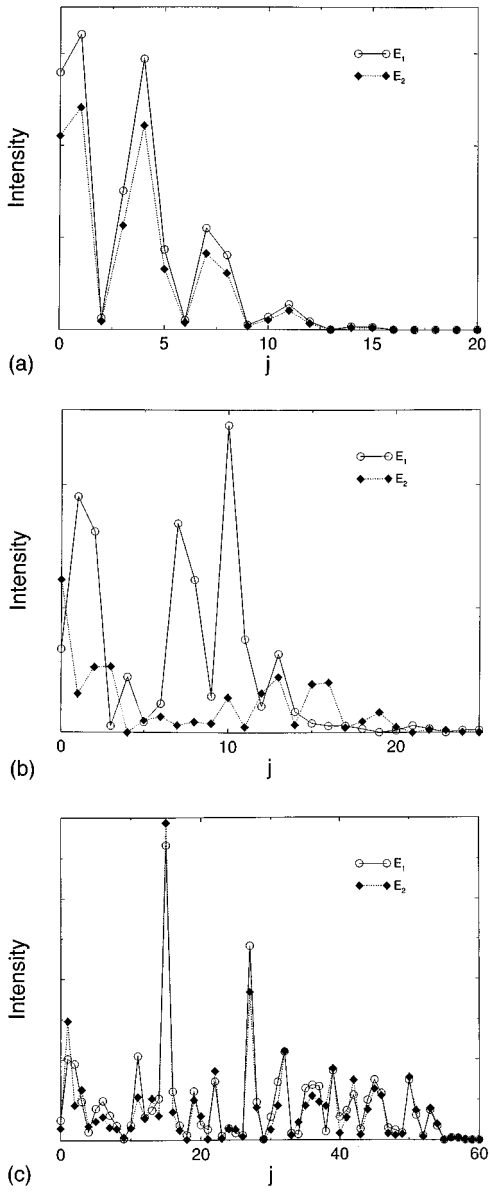

FIG. 7. (a) Rotational distributions $P_j(E)$ for BC ($ABC\rightarrow A+BC$), plotted vs the rotational quantum, j, of BC. The effective Hamiltonian parameters are $\rho=0.5/\mathrm{cm}^{-1}$, $M=100$, $N=1$ and an average resonance width $2\pi\sigma^2N=0.1$. The solid and dashed lines correspond to the energies $E_1=102$ and $E_2=104$ cm^{-1}, respectively. (b) The same for $N=8$ and $2\pi\sigma^2N=0.8$. (c) The same for $N=50$ and $2\pi\sigma^2N=5.0$.

The last equation clearly illustrates that for $N>1$, the dynamical coupling matrix elements connecting the different states of the activated complex to a particular final state j are superimposed with energy-dependent complex coefficients, so that state-specific information contained in $\{a_{j,n}\}$ is ''lost'' due to interference.

Figure 7(c) corresponds to a yet larger number of states of the activated complex ($N=50$). As in Fig. 7(b), the rotational distributions are again characterized by oscillations associated with the superposition of the dynamical coupling matrix elements. However, in contrast to the ''intermediate'' case (e.g., $N=8$), the distributions for the two neighboring energies are strongly correlated, resembling more the results of Fig. 7(a) for the limiting case $N=1$.

The increasing correlation of the rotational distributions at nearby values of E for increasingly larger N can be related to the increased degree of resonance overlap. The latter is a direct result of Eq. (2.7b), i.e.,

$$\langle\bar{\Gamma}\rangle\rho = 2\pi\sigma^2\rho N, \tag{4.16}$$

which implies that the degree of resonance overlap is linear in N. In the limit of nonoverlapping resonances, the widths ($\{\Gamma_l\}$) are typically smaller than the energy spacing between two nearby resonance energies. Consequently, for any energy E, one resonance (for which $E_l \approx E$) dominates the contribution to the summation over l in Eq. (4.15b). Moreover, each resonance state is well approximated by a specific molecular state, i.e., $u_m^{l'} \approx \delta_{l',m}$. Using these two approximations in Eq. (4.15b) one has

$$g_n(E_{l'}) \approx \text{const} \times \Phi_{0,l'} V_{l',n}, \tag{4.17}$$

which implies, according to Eq. (4.15a), that for a given photolysis energy E, $P_j(E)$ derives mainly from a single resonance state. When the difference between the two photolysis energies exceeds the average resonance width ($\langle\bar{\Gamma}\rangle$), each energy is likely to excite *a different resonance state*. Since the coupling matrix elements $\{V_{l',n}\}$ are random, the sum in Eq. (4.15a) will be different for each E, and consequently the rotational distributions will exhibit large sensitivity to the photolysis energy. For fixed (small) values of the density of states and the average coupling strength this situation is characteristic of small N's [i.e., small overlap according to Eq. (4.16)], as seen in Fig. 7(b) for $N=8$ and $\langle\bar{\Gamma}\rangle\rho = 0.4$. As N increases, the degree of resonance overlap increases so that at any photolysis energy a group of resonances typically dominates the summation in Eq. (4.15b) rather than a single resonance. In this case, two nearby photolysis energies which correspond approximately to excitation of the same group of resonances, will lead to a similar sum in Eq. (4.15a) and correlated rotational distributions. This situation is depicted in Fig. 7(c) for $N=50$ and $\langle\bar{\Gamma}\rangle\rho = 2.5$.

Before concluding this section we note that both the sudden and the random matrix approximations used in the present simulations tend to overestimate the sensitivity of the rotational distributions to the excitation energy for small N's. Within the sudden approximation, the couplings of specific final product states to the transition state (i.e., $\{a_{j,n}\}$) are sensitive to the specific level of the activated complex, n. In contrast, in cases where the dissociation dynamics is dominated by exit channel forces beyond the transition state (i.e., the sudden approximation does not apply), $\{a_{j,n}\}$ for different activated complex levels may be very similar. In this case the summation over different n-states in Eq. (4.15a) may lead to similar rotational distributions for nearby energies also for $N>1$.

The random matrix assumption (i.e., ergodic dynamics in the Q-space) leads to overestimation of the sensitivity of the rotational distributions to small changes in excitation energy, since the couplings of different resonance states to the activated complex [i.e., $\{V_{l',n}\}$ in Eq. (4.17)] are random. In reality, it is possible that the couplings of nearby resonance states to the activated complex will be correlated so that the coefficients $g_n(E)$ in Eq. (4.15a) will not change much for nearby energies, even when the resonances do not overlap. In this case energy sensitive distributions will not be observed.

Experimentally, the sensitivity of the rotational distributions to small changes in the excitation energy [e.g., Fig. 7(b)] is not expected to be observed for large molecules where the degree of resonance overlap increases rapidly with energy due to rapid increase in N. The energy sensitivity of the distributions is associated with an intermediate regime, in which N is large enough so that the dissociation dynamics is different for different activated complex states, and yet N is small enough so that the molecular resonances do not overlap appreciably. This is expected to be the case for small molecules with a tight transition state. Indeed, the measurements of Reisler and co-workers have shown that for the unimolecular decay of NO_2 in the range of 2000–3000 cm^{-1} above dissociation threshold, the NO rotational distributions obtained at nearby excitation energies are different.[7,8] *Ab initio* calculations[31] as well as variational RRKM calculations[24] confirm that the transition state of NO_2 tightens rapidly as the energy increases, which implies that N (as well as ρ and σ) is relatively small even high above the dissociation threshold.

In summary, fluctuations and oscillations in final state distributions are expected in almost every system with N larger than a few states, but their variations with small changes in E depend on the degree of overlap and the specific dynamics. Although the random matrix and the sudden approximations used here describe only specific limiting cases and real systems will display more complicated dynamics, we believe that the trends illustrated by the present simulations are representative of real systems.

V. DISCUSSION AND CONCLUSIONS

The work presented here, as well as that in our previous paper,[14] shows that a random matrix version of Feshbach's optical model provides a description of unimolecular reactions that is applicable *both to isolated and overlapping resonances*. Specifically, final state-selected spectra, distributions of decay widths and phases, the average decay width, and the unimolecular reaction rate can be described. Although the evolution of the system of resonances is treated as a scattering process, the physical interpretations of the state-selected spectral features, rates and product state distributions are couched in terms of statistical transition state theories. In particular, the resonances are assumed to evolve to final products via a ''bottleneck'' whose structure and energy levels are identified with the conventional transition state of statistical theories of unimolecular decay (e.g., PST, RRKM).

An important advantage of the formalism presented here is its ability to treat both loose and tight transition states. The evolution of the system up to the transition state is treated by using random coupling matrix elements and does not necessitate knowledge of the PES. However, from the transition state onward, the evolution is controlled by the dynamics on each PES, and the formalism presented here includes explicitly the dynamical coupling matrix elements. We point out also that the model is valid as long as a partitioning into the

bound (Q) and continuum (P) parts is possible, i.e., for dissociation that is not too fast.

The main assumption of the model lies in the use of the random matrix formalism, namely the coupling matrix elements between the quasibound states of the excited molecule and the transition state are random and can be chosen from a Gaussian (normal) distribution. This assumption is justified in cases when the states of the excited molecule are mixed (ergodic). Thus, the same assumption, i.e. complete intramolecular vibrational redistribution (IVR), that justifies the use of statistical theories in describing unimolecular decay, also provides the rationale behind assigning each resonance an equal, but random, probability for accessing all states of the transition state. In statistical theories, due to inherent ensemble averaging, resonance-specific effects are expected to wash out. In the cases discussed here, where the initial and final states are well defined, averaging is minimized and the assumption of random coupling matrix elements leads, for a loose transition state, to random fluctuations in the final state-selected spectra and product distributions. However, since each molecule has well defined resonance structures and dissociates on a specific PES, in reality the coupling matrix elements are resonance and molecule specific. Thus, the model described here is general in that it shows features that provide guidelines in interpreting results of state-selected experiments in the presence of overlapping resonances, but it is not intended to be applied quantitatively to a specific molecule.

The main results derived from the model and their interpretations are summarized below:

(1) For isolated resonances or at low level of overlap, the distribution of decay widths obeys a χ^2-like distribution and the phases are clustered around the real axis. With increasing overlap, the distribution of decay widths starts to broaden and deviates from that predicted by a χ^2-like distribution, while the phases become randomly distributed. This leads to interference, and for a molecule with a low density of states, to the observation of spectral features that depend sensitively on the monitored final state. When the density of states becomes large or many initial or final states are summed, the spectral features become smeared and the conditions which justify the random phase approximation prevail.

(2) When the resonances overlap, there is no simple relation between the resonance widths (which cannot be observed experimentally), the widths of the spectral structures, and the average rate. The simulations, which allow independent variation of the average width and rate, can be optimized until best agreement with the experiment is obtained. The average width can be extracted by simulating the experimental spectra, and the average rate can be calculated using Eq. (2.9). The relation between the average rate and width in the case of overlapping resonances is discussed in detail elsewhere.[14]

(3) For a loose transition state, the number of final states is equal to N, the number of transition state levels, and the simulations can be compared directly (albeit qualitatively) with experimental final state-selected spectra. For example, when ρ and N are known, the average width can be extracted by simulating the spectra. The simulated final state-selected spectra are shown to be qualitatively similar to those observed in the near-threshold unimolecular reaction of NO_2 by monitoring selected levels of NO.[4] Both experiments and simulations show spectra that differ in line intensities, positions, and widths when different final states are monitored. Our model also predicts trivially that the rotational state distributions at specific photolysis energy will show random fluctuations.

(4) Simulations were also carried out for dissociation over a barrier (i.e., with a tight transition state). The transition state was modeled with hindered rotor wave functions, and a limiting case where no final state interactions occur beyond the transition state was treated explicitly (i.e., by using the Franck–Condon model for dissociation). In this case, the behavior of the rotational state distributions depends on the excess energy regime. When a modest number of transition state levels are populated (e.g., 5–20), prominent oscillatory structures appear in the rotational distributions, which change sensitively with a small change in photolysis energy. The behavior obtained in this regime is quite similar to that seen in the unimolecular reaction of NO_2 at excess energies 2000–3000 cm^{-1}, where large oscillations in the NO rotational distributions that change significantly with a small changes in photolysis energy (e.g., 5–50 cm^{-1}) are observed.[8] When a large number of transition state levels are populated, the simulated oscillatory structures do not depend sensitively on photolysis energy any more. In this regime, the degree of overlap is very large and a true statistical limit is reached. Here, averaging over even few initial states will tend to smooth the oscillations.[28,32]

ACKNOWLEDGMENTS

H. R. would like to thank W. H. Miller and C. B. Moore for the hospitality during her Sabbatical stay at Berkeley, and S. A. Reid for many useful discussions. U. P. thanks the Fulbright and the Rothschild foundations for postdoctoral fellowships. This work was supported by the director, Office of Energy Research, Office of Basic Energy Sciences, Chemical Sciences Division of the U.S. Department of Energy under Contract Nos. DE-AC03-76SF00098 (to W.H.M.) and DE-FG03-88ER13959 (to H.R.).

[1] H. Reisler and C. Wittig, Annu. Rev. Phys. Chem. **37**, 307 (1986), and references therein; in *Advances in Kinetics and Dynamics*, edited by J. R. Barker (JAI, Greenwich, 1992), Vol. 1; W. H. Green, Jr., C. B. Moore, and W. F. Polik, Annu. Rev. Phys. Chem. **43**, 307 (1992).

[2] W. F. Polik, C. B. Moore, and W. H. Miller, J. Chem. Phys. **89**, 3584 (1988); W. F. Polik, D. R. Guyer, C. B. Moore, and W. H. Miller, *ibid*. **92**, 3471 (1990); W. H. Miller, R. Hernandez, and C. B. Moore, *ibid*. **93**, 5657 (1990); R. Hernandez, W. H. Miller, C. B. Moore, and W. F. Polik, *ibid*. **99**, 950 (1993).

[3] L. D. Landau and E. M. Lifshitz, *Quantum Mechanics* (Pergamon, London, Paris, 1958), pp. 440–441.

[4] J. Miyawaki, K. Yamanouchi, and S. Tsuchiya, J. Chem. Phys. **99**, 254 (1993).

[5] S. I. Ionov, H. F. Davis, K. Mikhaylichenko, L. Valachovic, R. A. Beaudet, and C. Wittig, J. Chem. Phys. **101**, 4809 (1994).

[6] C. X. W. Qian, A. Ogai, H. Reisler, and C. Wittig, J. Chem. Phys. **90**, 209 (1989).

[7] D. C. Robie, M. Hunter, J. L. Bates, and H. Reisler, Chem. Phys. Lett. **193**, 413 (1992); M. Hunter, S. A. Reid, D. C. Robie, and H. Reisler, J. Chem. Phys. **99**, 1093 (1993).
[8] S. A. Reid, J. T. Brandon, M. Hunter, and H. Reisler, J. Chem. Phys. **99**, 4860 (1993); S. A. Reid, D. C. Robie, and H. Reisler, *ibid*. **100**, 4256 (1994); S. A. Reid and H. Reisler, *ibid*. **101**, 5683 (1994).
[9] U. Robra, H. Zacharias, and K. H. Welge, Z. Phys. D **16**, 175 (1990).
[10] N. Changlong, L. Hua, and J. Pfab, J. Phys. Chem. **97**, 7458 (1993).
[11] T. Ericson, Ann. Phys. **23**, 390 (1963); Phys. Rev. Lett. **5**, 430 (1960).
[12] J. R. Taylor, *Scattering Theory* (Wiley, New York, 1972).
[13] H. Feshbach, *Theoretical Nuclear Physics* (Wiley, New York, 1992); R. D. Levine, *Quantum Mechanics of Molecular Rate Processes* (Clarendon, Oxford, 1969).
[14] U. Peskin, H. Reisler, and W. H. Miller, J. Chem. Phys. **101**, 9672 (1994).
[15] I. Rotter, Rep. Prog. Phys. **54**, 635 (1991); W. Iskra, I. Rotter, and F.-M. Dittes, Phys. Rev. C **47**, 1086 (1993); K. Someda, H. Nakamura, and F. H. Mies, Chem. Phys. **187**, 195 (1994); Prog. Theor. Phys. Suppl. **116**, 443 (1994).
[16] (a) M. D.-Lecomte and F. Culot, J. Chem. Phys. **98**, 7819 (1993); (b) F. Remacle and R. D. Levine, J. Phys. Chem. **95**, 7124 (1991); R. Remacle, J. C. Lorquet, and R. D. Levine, Chem. Phys. Lett. **209**, 315 (1993).
[17] A. Delon and R. Jost, J. Chem. Phys. **95**, 5686 (1991); **95**, 5700 (1991); G. Persch, E. Mehdizadeh, W. Demtrder, Th. Zimmermann, H. Koppel, and L. S. Cederbaum, Ber. Bunsenges. Phys. Chem. **92**, 312 (1988).
[18] P. J. Robinson and K. A. Holbrook, *Unimolecular Reactions* (Wiley, New York, 1972); W. Forst, *Theory of Unimolecular Reactions* (Academic, New York, 1973).
[19] N. Moiseyev, in *The Letroped Symposium View on a Generalized Inner Product*, Lecture Notes in Physics, edited by E. Brandas and N. Elander (Springer, Berlin, 1989), Vol. 211.
[20] P. Pechukas, J. C. Light, and C. Rankin, J. Chem. Phys. **44**, 794 (1966); P. Pechukas and J. C. Light, *ibid*. **42**, 3281 (1965); J. C. Light, Discuss. Faraday Soc. **44**, 14 (1967).
[21] R. D. Levine, Ber. Bunsenges. Phys. Chem. **92**, 222 (1988).
[22] R. Schinke, *Photodissociation Dynamics* (Cambridge University, Cambridge, 1993).
[23] D. M. Wardlaw and R. A. Marcus, Adv. Chem. Phys. **70**, 231 (1988), and references therein.
[24] S. J. Klippenstein and T. Radivoyevitch, J. Chem. Phys. **99**, 3644 (1993).
[25] S. J. Klippenstein, in *Advances in Physical Chemistry: The Chemical Dynamics and Kinetics of Small Radicals*, edited by K. Liu and A. F. Wagner (World Scientific, Singapore, 1994).
[26] J. A. Beswick and W. M. Gelbart, J. Phys. Chem. **84**, 3148 (1980).
[27] M. D. Morse and K. F. Freed, J. Chem. Phys. **74**, 4395 (1981); **78**, 6045 (1983); Chem. Phys. Lett. **74**, 49 (1980); M. D. Morse, K. F. Freed, and Y. B. Band, J. Chem. Phys. **70**, 3064 (1979); **70**, 3620 (1979); K. F. Freed and Y. B. Band, in *Excited States*, edited by E. Lim (Academic, New York, 1978), Vol. 3.
[28] H. Reisler, H.-M. Keller, and R. Schinke, Comments At. Mol. Phys. (in press).
[29] H. Grinberg, C. J. Williams, and K. F. Freed, J. Chem. Phys. **100**, 9215 (1994).
[30] C. X. W. Qian, A. Ogai, J. Brandon, Y. Y. Bai, and H. Reisler, J. Phys. Chem. **95**, 6763 (1991).
[31] H. Katagiri and S. Kato, J. Chem. Phys. **99**, 1 (1993).
[32] S. A. Reid and H. Reisler (unpublished).